JOURNAL OF Materials CHEMISTRY

The hydrothermal synthesis of the new manganese and vanadium oxides, $NiMnO_3H$, MAV_3O_7 and $MA_{0.75}V_4O_{10}\cdot 0.67H_2O$ ($MA = CH_3NH_3$)†

Rongji Chen,[a] Peter Y. Zavalij,[a] M. Stanley Whittingham,[a] John E. Greedan,[b] N. P. Raju[b] and Mario Bieringer[b]

[a]*Chemistry Department and Materials Research Center, State University of New York at Binghamton, Binghamton, NY 13902–6000, USA. E-mail: stanwhit@binghamton.edu*
[b]*Department of Chemistry and Brockhouse Institute for Materials Research, McMaster University, Hamilton, Ontario, Canada L8S 4M1*

Received 6th April 1998, Accepted 8th July 1998

The hydrothermal reaction of manganese or vanadium oxides in the presence of organic cations leads to the formation of new layered structures. When nickel salts are hydrothermally reacted with tetramethylammonium permanganate a new orthorhombic form of nickel manganese oxide, $NiMnO_3H_x$ (where $x \leqslant 1$) is formed. It readily chemically intercalates lithium; it has space group $Cmc2_1$, $a = 2.861(1)$ Å, $b = 14.650(1)$ Å, and $c = 5.270(1)$ Å. The magnetic properties of this compound are quite different from the ilmenite $NiMnO_3$ phase, showing paramagnetism above 390 K and more complex behavior below that temperature. The hydrothermal reaction of vanadium pentoxide with methylamine leads to a series of new layered vanadium oxides, which differ in structure from the corresponding ones prepared in the presence of the tetramethylammonium ion because of the existence of hydrogen bonding. Methylamine is the first organic to form a double sheet vanadium oxide, $(CH_3NH_3)_{0.75}V_4O_{10}\cdot 0.67H_2O$, with the δ-$Ag_xV_2O_5$ structure. $(CH_3NH_3)_{0.75}V_4O_{10}\cdot 0.67H_2O$ is monoclinic, space group $C2/m$ with $a = 11.673(1)$ Å, $b = 3.668(1)$ Å, $c = 11.095(1)$ Å and $\beta = 99.865(5)^\circ$. $(CH_3NH_3)V_3O_7$ shows significant buckling of the layers compared with $N(CH_3)_4V_3O_7$, and has a monoclinic unit cell, space group $P2_1/c$ with $a = 11.834(8)$ Å, $b = 6.663(4)$ Å, $c = 15.193(9)$ Å and $\beta = 138.104(1)^\circ$.

Introduction

There has been much interest recently in the synthesis and characterization of new materials by soft chemistry approaches,[1] because such materials tend to exhibit different properties and to be more chemically reactive than materials formed at higher temperatures. Whereas the latter tend to be the thermodynamically stable phases, soft chemistry approaches that often take place under kinetic conditions can lead to new metastable phases. These phases may be layered, or contain tunnels, into which ions or molecules may be intercalated allowing their physical properties to be modified, or by appropriate choice of tunnel size making them chemically selective. Moreover, such compounds may be selectively reactive, being very reactive to some ions such as lithium ions under ambient conditions, yet despite being highly oxidizing being relatively inert to their surroundings.

Intercalation and ion-exchange reactions are soft-chemistry approaches to modifying an already existing crystalline lattice, or amorphous compound. Such transformations can be performed by direct chemical reaction or in an electrochemical cell. Hydrothermal or solvothermal synthesis is an approach to build a structure from scratch by precipitation from an aqueous or non-aqueous medium above the solvent's normal boiling point. Hydrothermal synthesis under mild conditions, normally autogeneous pressure and $\leqslant 200\,^\circ$C, has received extensive study particularly in the last decade for the formation of zeolites,[2] vanadium and molybdenum phosphates[3,4] and simple transition metal oxides such as tungsten oxide.[5–8]

Previously we reported the formation of tungsten oxides and showed how by changing the pH it was possible to form either a hexagonal or a pyrochlore tunnel structure.[6] Subsequently, tunnel compounds of molybdenum trioxide were synthesized[9] and MoO_3 with empty tunnels was prepared for the first time.[10] In each of the above cases, the oxidation state of the transition metal is maintained during reaction. However, when aqueous permanganate solutions are heated to 170 °C, the manganese is reduced and the layered compounds, $M_yMnO_2\cdot nH_2O$ where M = Li, Na, K, and Rb are formed.[11–13] These have the same structure as $Li_xTiS_2\cdot nH_2O$[14] and are under study for lithium battery cathodes.[15]

Traditionally, structure directing agents are added to the hydrothermal reaction medium so as to provide a degree of control over the structure formed. This approach has been remarkably successful, leading for example to a whole series of zeolites with well defined tunnel sizes from that of ZSM-5 to the *ca.* 40 Å tunnels found in MCM-41.[16] When small organic cations, such as tetramethylammonium, $N(CH_3)_4^+$ = TMA, are added to tungsten oxide solutions large cluster tungstates are formed.[17] However, in the case of molybdenum oxide, the compound $TMAMo_4O_{12}$ was formed;[18] this has a new layer structure with the TMA ions between the layers. TMA was also used[19] to form a new layered titanium phosphate that readily underwent ion-exchange reactions.

TMA has been extensively studied[19,20] and in the case of vanadium oxides at least seven phases have been formed, exclusive of clusters which are also readily formed. The phase formed depends on the ratio of reactants present and critically on the pH of the reaction medium. Fig. 1 shows some of the

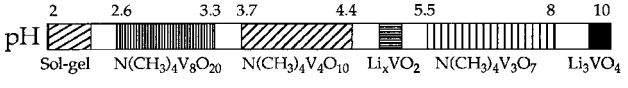

Fig. 1 Phases formed as a function of pH when V_2O_5, TMA and LiOH are reacted at 185 °C.

†Basis of the presentation given at Materials Chemistry Discussion No. 1, 24–26 September 1998, ICMCB, University of Bordeaux, France.

phases formed as a function of pH.[21–23] In addition, Nazar *et al.*[24] have reported the formation of an intriguing $TMA_5V_{18}O_{46}$ intergrowth phase which has not yet been found in our synthesis. To obtain the pure phases noted in Fig. 1, it is desirable to buffer the pH, so that it does not change during the reaction otherwise the phase formed is a function of the reaction time. We have found that acetic acid forms an effective buffer in the presence of the tetramethylammonium ion. Stronger acids, for example oxalic and mineral acids, are partially consumed during the reaction leading to pH changes.

There are a number of trends that can be identified from Fig. 1. At the higher pH values, the vanadium is only present as tetrahedra. As the pH is reduced the coordination becomes square pyramidal with the characteristic V=O at the apex of the pyramid, and at the lowest pH values distorted octahedral. Thus, one can predetermine the vanadium coordination by controlling the pH of the reaction medium. The species in aqueous solution also show similar coordination trends with pH, and Livage[25] has proposed a mechanism for their condensation leading to layered structures. Where TMA is retained in the structure, its content increases with increase of pH; this can be related to the decreasing density of vanadium species per unit area of interlayer region as the pH increases.

The TMA cation has been the most studied structure directing ion, or templating ion, particularly for vanadium oxides. It acts as a large spherical cation, unlike for example ethylenediamine, DABCO, *etc.* which can be ionic or chelating depending on the metal species present and the pH of the reaction medium. A prevalent structural type is that of V_6O_{14}, exemplified by $TMAV_3O_7$. It is also formed by $(DABCO)V_6O_{14}$,[26,27] $Zn(en)_2V_6O_{14}$,[28] and $Ni(en)_2V_6O_{14}$[29] and will be discussed further later.

In this paper we will discuss what happens when the TMA cation is replaced by the methylammonium cation, $CH_3NH_3^+$, in the formation of vanadium oxides. The methylammonium ion, $CH_3NH_3^+$, unlike the tetramethylammonium ion, should allow for hydrogen bonding between the amine hydrogens and the oxygen in the vanadium oxide matrix. In addition, there is the possibility of bonding between the nitrogen lone pair and the vanadium atom, which is often found in these structures in square pyramidal coordination with only weak bonding opposite the apical vanadyl bond. We will also discuss what happens when tetramethylammonium permanganate, $(CH_3)_4NMnO_4$, is hydrothermally reacted in the presence of nickel cations.

Experimental

Two layered vanadium oxides were hydrothermally synthesized by dissolving V_2O_5 powder from Johnson & Matthey in methylamine aqueous solution from Fisher Scientific in a 1:2 molar ratio. After adjusting the pH with acetic acid in one case to 4 and in the other to 7, the final solution was transferred to a 125 ml Teflon lined autoclave (Parr bomb), sealed, and reacted hydrothermally for 4 or 5 days at 200 °C. The oxidation state of the vanadium was determined by $Ce(SO_4)_2 \cdot H_2SO_4$ oxidization, the nitrogen content by the Kjeldahl method and the vanadium content by complete combustion to V_2O_5 on a Perkin Elmer TGA 7 in flowing oxygen.

The nickel manganese oxide was synthesized by reacting hydrothermally for 2 days at 200 °C a mixture of 0.001 moles $N(CH_3)_4MnO_4$, 0.0015 moles $Ni(OOCCH_3)_2 \cdot 4H_2O$ and 0.001 moles Li_2CO_3 in 25 ml water. The crystals formed were filtered and washed with 2 M HNO_3 to remove any $Ni(OH)_2$ impurity. The $N(CH_3)_4MnO_4$ starting material was synthesized by mixing together, in a 1:1 molar ratio, separate aqueous solutions of $N(CH_3)_4Cl$ and $KMnO_4$; $N(CH_3)_4MnO_4$ precipitated immediately. The reader is warned that tetramethylammonium permanganate is potentially explosive and should not be heated in the dry state, as for example on a TGA.

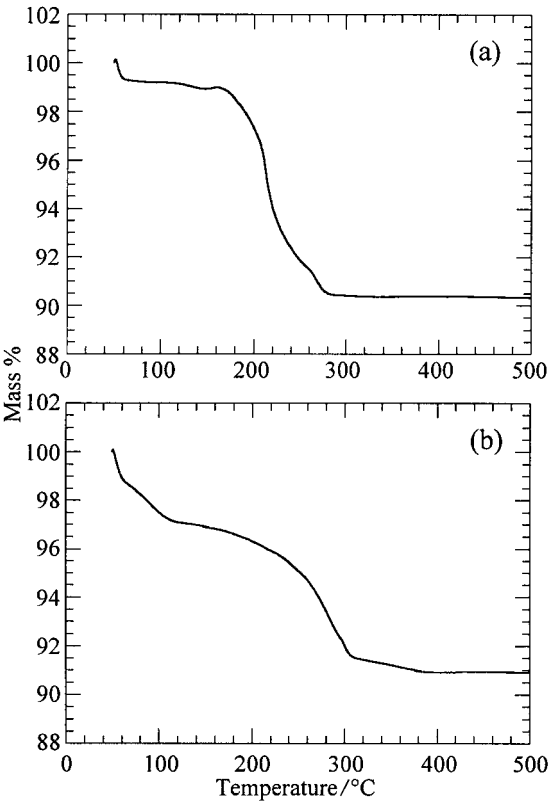

Fig. 2 Thermogravimetric analysis of (a) $(CH_3NH_3)V_3O_7$, and (b) $(CH_3NH_3)_{0.75}V_4O_{10} \cdot 0.67H_2O$.

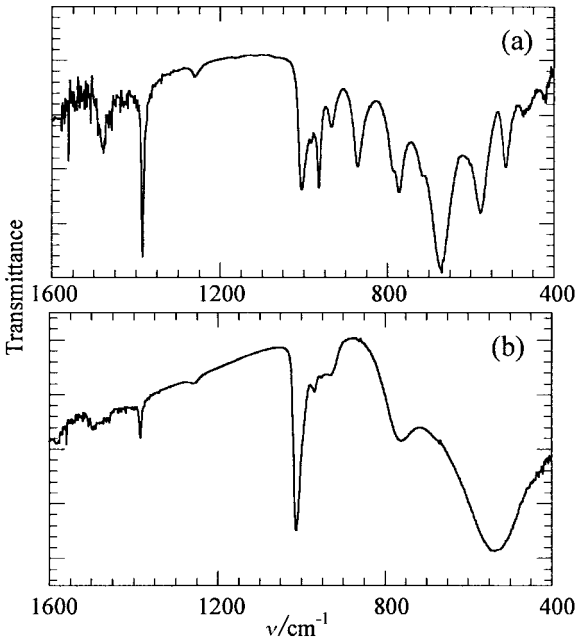

Fig. 3 FTIR spectra of (a) $(CH_3NH_3)V_3O_7$, and (b) $(CH_3NH_3)_{0.75}V_4O_{10} \cdot 0.67H_2O$.

The reactivity with lithium was determined by reaction with *n*-butyllithium from Aldrich Chemicals in a dry box. Electrochemical studies were conducted in lithium cells using $LiAsF_6$ in PC:DME=1:1 as the electrolyte; a MacPile potentiostat was used to cycle the cells. The TGA were obtained on a Perkin-Elmer model TGA 7, the FTIR spectra on a Perkin-Elmer 1600 series, and the electron microprobe analysis on a JEOL 8900.

Table 1 Crystallographic data for $(CH_3NH_3)V_3O_7$ and $(CH_3NH_3)_{0.75}V_4O_{10}\cdot 0.67H_2O$

Formula	$(CH_3NH_3)V_3O_7$		$(CH_3NH_3)_{0.75}V_4O_{10}\cdot 0.67H_2O$	
Z	4		4	
Space group	$P2_1/c$		$C2/m$	
a/Å	11.8343(8)		11.6728(3)	
b/Å	6.6636(4)		3.6681(1)	
c/Å	15.1930(9)		11.0949(3)	
β/°	138.104(1)		99.865(5)	
Cell volume/Å^3	800.1(2)		468.03(5)	
$F(000)$	576 **e**		381 **e**	
Calculated density/g cm^{-3}	2.465		2.8212	
Absorption coefficient/cm^{-1}	36.29		351.65	
Experimental data	Single crystal		Powder	
Diffractometer	Siemens Smart CCD		Scintag XDS2000	
Radiation, wavelength/Å	Mo-Kα, 0.71069		Cu-Kα, 1.54178	
Restrictions	$F_{hkl}>4\sigma(F)$			
Weighting scheme	$[\sigma(F)^2+0.0004F_{obs}{}^2]^{-1}$		$1/Y_{obs}$	
Peak shape function			pseudo-Voigt	
Preferred orientation			$(\tau\cos^2\phi+\sin^2\phi)^{-1/2}$	
Refined parameters	133		34	
2θ(max)/°	56.4		68.7	
Measured reflections	5103		93 integrated intensities	
Unique reflections	1864		127	
Refined reflections	1756		127	
R-factors	R(sig)	0.023	$R(B)$	0.059
	R(eq)	0.066	R(exp)	0.080
	$R(F)$	0.045	$R(p)$	0.091
	$Rw(F)$	0.051	$Rw(p)$	0.123

Table 2 Distances (Å) and angles (°) for $(CH_3NH_3)V_3O_7$ and $(CH_3NH_3)_{0.75}V_4O_{10}\cdot 0.67H_2O$

$(CH_3NH_3)V_3O_7$

Corner SP		Middle SP		Tetrahedron	
Distance/Å, Angle/°		Distance/Å, Angle/°		Distance/Å, Angle/°	
V1=O1	1.614(5)	V2=O2	1.611(4)	V3=O3	1.611(3)
V1–O5′	1.898(3)	V2–O4	1.929(5)	V3–O4	1.706(6)
V1–O5	1.922(4)	V2–O5	1.933(4)	V3–O6′	1.790(3)
V1–O7	1.993(4)	V2–O7′	1.972(3)	V3–O7″	1.815(4)
V1–O6	2.022(3)	V2–O6	1.991(3)		
O1=V1–O5′	111.8(2)	O2=V2–O4	106.6(2)	O3=V3–O4	110.1(2)
O1=V1–O5	114.3(2)	O2=V2–O5	112.9(2)	O3=V3–O6′	107.4(2)
O1=V1–O7	102.2(2)	O2=V2–O7′	105.2(2)	O3=V3–O7″	108.0(2)
O1=V1–O6	104.2(2)	O2=V2–O6	106.7(2)	O4–V3–O6′	109.8(2)
O5′–V1–O5	133.8(2)	O4–V2–O5	140.4(2)	O4–V3–O7″	111.5(2)
O5′–V1–O7	82.6(2)	O4–V2–O7′	89.9(2)	O6′–V3–O7″	110.1(2)
O5′–V1–O6	89.6(2)	O4–V2–O6	89.1(2)		
O5–V1–O7	90.1(2)	O5–V2–O7′	82.2(2)		
O5–V1–O6	77.2(2)	O5–V2–O6	77.7(2)		
O7–V1–O6	153.5(2)	O7′–V2–O6	146.9(2)		

$(CH_3NH_3)_{0.75}V_4O_{10}\cdot 0.67H_2O$

Octahedron V1		Octahedron V2	
V1=O5	1.64(1)	V2=O3	1.59(1)
V1–O1	1.87(2)	V2–O1′	1.78(2)
V1–O4′	1.91(1)	V2–O2′	1.87(1)
V1–O4″	1.91(1)	V2–O2″	1.87(1)
V1–O2	2.09(2)	V2–O4	1.98(2)
V1···O4*	2.59(1)	V2···O1″	2.47(1)
O5=V1–O1	101.4(5)	O3=V2–O1′	102.5(6)
O5=V1–O4′	102.2(5)	O3=V2–O2′	98.4(6)
O5=V1–O4″	102.2(5)	O3=V2–O2″	98.4(6)
O5=V1–O2	101.3(5)	O3=V2–O4	104.7(5)
O5=V1···O4*	176.4(5)	O3=V2···O1″	178.8(5)
O1–V1–O4′	98.1(5)	O1′–V2–O2′	95.1(6)
O1–V1–O4″	98.1(5)	O1′–V2–O2″	95.1(6)
O1–V1–O2	157.3(5)	O1′–V2–O4	152.8(5)
O1–V1···O4*	75.0(4)	O1′–V2···O1″	76.3(5)
O4′–V1–O4″	147.3(5)	O2′–V2–O2	158.0(6)
O4′–V1–O2	77.0(5)	O2′–V2–O4	81.1(5)
O4′–V1···O4*	78.5(5)	O2′–V2···O1″	81.8(5)
O4″–V1–O2	77.0(5)	O2″–V2–O4	81.1(5)
O4″–V1···O4*	78.5(5)	O2″–V2···O1″	81.8(5)
O2–V1···O4*	82.3(5)	O4–V2···O1″	76.5(4)

O5′ $1-x$, $1/2+y$, $3/2-z$, O6′ $1-x$, $1-y$, $1-z$, O7′ $1-x$, $-1/2+y$, $3/2-z$, O7″ x, $1/2-y$, $-1/2+z$, O4′ $1/2+x$, $1/2+y$, z, O4″ $1/2+x$, $-1/2+y$, z, O4* $1-x$, y, $-z$, O1′ $-1+x$, y, z, O2′ $-1/2+x$, $1/2+y$, z, O2″ $-1/2+x$, $-1/2+y$, z, O1″ $1-x$, y, $-z$.

The structure determination was done on a Scintag XDS 2000 powder θ–θ diffractometer, a Siemens Smart CCD single crystal X-ray diffractometer at Syracuse University and the neutron diffractometer at McMaster University using $\lambda =$ 1.3920 Å neutrons. All crystallographic refinement was conducted using the CSD (Crystal Structure Determination)[30] and GSAS (General Structure Analysis System)[31] packages. Magnetic susceptibility data were collected using a SQUID magnetometer (Quantum Design).

Results and discussion

Methylammonium vanadium oxides

Two different products were obtained depending on the initial pH of the reaction medium, which was set by the addition of acetic acid. For an initial pH of 4, dark green clay-like $(CH_3NH_3)_{0.75}V_4O_{10}\cdot 0.67H_2O$ was obtained, and the pH after reaction was 4.5. For an initial pH of 7, large dark brown plate-like crystals of $(CH_3NH_3)V_3O_7$ were obtained; the final pH was 7 after reaction. The oxidation states of the vanadium in $(CH_3NH_3)V_3O_7$, and $(CH_3NH_3)_{0.75}V_4O_{10}\cdot 0.67H_2O$, were 4.34 and 4.82 respectively. The nitrogen content was consistent with the organic content measured by complete combustion to V_2O_5. The thermal analyses of these compounds under oxygen at a heating rate of 3 °C min^{-1} are shown in Fig. 2. $(CH_3NH_3)V_3O_7$ loses 1% of adsorbed surface water first, then above 160 °C, CH_3NH_2 burns off and oxygen is taken up to fully oxidize the vanadium to V_2O_5 at 300 °C. The total weight loss is 8.5% which matches very well with the theoretical calculation. Thermal decomposition of the $(CH_3NH_3)_{0.75}V_4O_{10}\cdot 0.67H_2O$ compound under O_2 indicates 3% water loss followed by a 6% CH_3NH_2 loss before it converts to V_2O_5. All the residues after thermal analysis are orange and their X-ray diffraction patterns show the presence of pure V_2O_5. The methylamine burns off earlier than observed with the tetramethylammonium ion, which is not lost until 300 °C.[22]

The FTIR spectrum of vanadium pentoxide shows three peaks at 1021 cm^{-1}, 827 cm^{-1} and 617 cm^{-1}, which can be associated with the V=O and two V–O vibrations, one bridging (900–700 cm^{-1}) and the other (800–400 cm^{-1}) to oxygens in chain positions between three vanadiums. Both new compounds [Fig. 3(a)–(b)] not only have vanadium and oxygen bond vibration peaks (below 1100 cm^{-1}), but also have a peak at 1382 cm^{-1}, which belongs to the C–N vibration from the CH_3NH_3. The rich spectrum of $(CH_3NH_3)V_3O_7$ is reminiscent of that of $TMAV_3O_7$,[22] suggesting that both VO_5 square pyramids and VO_4 tetrahedra are present in the structure. The relatively simple spectrum of $(CH_3NH_3)_{0.75}V_4O_{10}\cdot 0.67H_2O$ has many similarities to that of the δ-V_2O_5 phase $Zn_{0.4}V_2O_5$ reported by us earlier,[32] and which contains only distorted VO_6 octahedra.

The powder diffraction pattern of $(CH_3NH_3)V_3O_7$ was indexed with monoclinic symmetry, space group $P2_1/c$ with lattice parameters $a = 11.834(8)$ Å, $b = 6.663(4)$ Å, $c = 15.193(9)$ Å and $\beta = 138.104(1)°$. $(CH_3NH_3)_{0.75}V_4O_{10}\cdot 0.67H_2O$ also has monoclinic symmetry, space group $C2/m$ with lattice parameters $a = 11.6728(3)$ Å, $b = 3.6681(1)$ Å, $c = 11.0949(3)$ Å and $\beta = 99.865(1)°$. The crystallographic data are given in Tables 1, 2 and 3. Full crystallographic details, excluding structure factors, have been deposited at the Cambridge Crystallographic Data Centre (CCDC). See Information for Authors, Issue 1. Any request to the CCDC for this material should give the full literature citation and the reference number 1145/111.

The structure of $(CH_3NH_3)V_3O_7$ was solved using single crystal techniques, whilst that of $(CH_3NH_3)_{0.75}V_4O_{10}\cdot 0.67H_2O$ was solved using Rietveld powder methods. Both structures contain vanadium oxide layers between which reside the methylammonium ions, as shown in Fig. 4. The former contains a single sheet of vanadium oxide in which the vanadium resides in both square-pyramidal (SP) and tetrahedral (T) coordination, whereas the latter has a bi-layer of

Table 3 Atomic parameters for $(CH_3NH_3)V_3O_7$ and $(CH_3NH_3)_{0.75}V_4O_{10}\cdot 0.67H_2O$

$(CH_3NH_3)V_3O_7$					
Atom	x/a	y/b	z/c	B(iso/eq)[a]	Occupation
V1	0.58670(8)	0.4723(1)	0.78436(6)	0.74(4)[a]	
V2	0.33968(8)	0.24144(9)	0.52840(6)	0.72(4)[a]	
V3	0.58584(9)	0.25999(9)	0.48618(7)	0.72(4)[a]	
O1	0.7707(4)	0.4178(4)	0.8517(3)	1.3(2)[a]	
O2	0.1374(4)	0.2712(4)	0.4093(3)	1.4(2)[a]	
O3	0.7506(4)	0.2897(4)	0.6427(3)	1.4(2)[a]	
O4	0.4117(4)	0.2202(4)	0.4492(3)	1.2(2)[a]	
O5	0.4325(4)	0.2495(4)	0.6999(3)	1.0(2)[a]	
O6	0.4410(4)	0.5148(4)	0.5921(3)	0.9(2)[a]	
O7	0.6251(4)	0.4505(4)	0.9359(3)	1.0(2)[a]	
N	0.0336(5)	0.1322(6)	0.6639(4)	1.5(2)[a]	
C	0.0564(7)	0.3229(8)	0.6276(5)	2.1(3)[a]	
H1n	−0.064(6)	0.077(7)	0.600(4)	0.9(8)	
H2n	0.047(8)	0.170(11)	0.730(6)	4.5(15)	
H3n	0.095(8)	0.018(9)	0.685(6)	3.3(13)	
H1c	−0.018(10)	0.430(11)	0.607(7)	5.3(17)	
H2c	0.166(9)	0.395(10)	0.703(7)	4.1(15)	
H3c	0.074(11)	0.269(11)	0.566(8)	6.5(19)	
$(CH_3NH_3)_{0.75}V_4O_{10}\cdot 0.67H_2O$					
V1	0.7898(4)	0	0.1358(3)	0.9(2)	
V2	0.0906(5)	0	0.1356(4)	1.3(2)	
O1	0.9364(13)	0	0.0898(10)	1.2(4)	
O2	0.608(2)	0	0.1122(10)	3.3(4)	
O3	0.1052(10)	0	0.2806(11)	1.5(4)	
O4	0.2512(14)	0	0.1015(11)	2.2(4)	
O5	0.8244(11)	0	0.2855(11)	2.2(5)	
N	0.6919(15)	0	0.493(2)	6.2(6)	0.90(2)
C1	0.472(5)	0	0.450(3)	6.2(6)	0.52(2)
C2	0.929(3)	0	0.530(4)	6.2(6)	0.65(2)

[a] $B(\text{eq}) = 1/3(B_{11}a^{*2}a^2 + \ldots + 2B_{23}b^*c^*bc\cos\alpha)$.

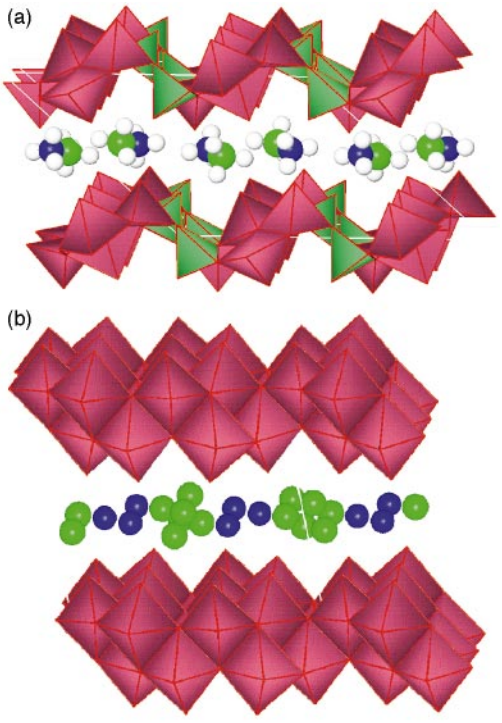

Fig. 4 The structures of (a) $(CH_3NH_3)V_3O_7$, and (b) $(CH_3NH_3)_{0.75}V_4O_{10}\cdot 0.67H_2O$.

vanadium oxide with the vanadium in a distorted octahedron. So, just as noted for the tetramethylammonium ion[23] the vanadium coordination number increases with decrease of the pH of the reaction medium.

The V_3O_7 layers in $(CH_3NH_3)V_3O_7$ contain chains made by edge sharing of VO_5 square pyramids, as indicated in Fig. 5;

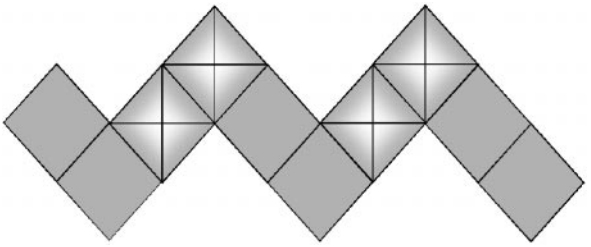

Fig. 5 Edge sharing of VO_5 square pyramids to form zig-zag chains, ☒ apex up, □ apex down.

Table 4 Relationship between the four V_3O_7 structures

Symmetry relations between SP_2T chains	Corner of tetrahedron shared between chains	
	Top (→tilted layer)	Bottom (→flat layer)
Glide plane	$(CH_3NH_3)V_3O_7$ $t=7.597$ Å, $c=2t$	$(en_2M)V_6O_{14}$ $t=7.851$ Å, $c=2t$
Translation	$(DABCO)V_6O_{14}\cdot H_2O$ $t=7.574$ Å, $c=t$	$TMAV_3O_7$ $t=8.427$ Å, $c=t$

their apices alternate two up, then two down. There are two types of square pyramids (SP)—corner SP that shares two edges next to each other and middle SP that shares opposite edges. The vanadyl oxygen at the SP apex is not shared. The chains are joined into layers by corner shared tetrahedra (T). Each tetrahedron shares two corners with one chain and one with another, one corner remains free. There is significant hydrogen bonding in $(CH_3NH_3)V_3O_7$ with the methylammonium cations making four hydrogen bonds N–H···O with lengths from 2.88 to 3.03 Å whereas the length of the four contacts C–H···O range from 3.24 to 3.33 Å. This hydrogen bonding causes significant buckling of the V_3O_7 sheets as compared with those of $TMAV_3O_7$.[33]

The V_3O_7 layer in $(CH_3NH_3)V_3O_7$ is compared in Fig. 6 to those found in other vanadium oxide compounds $(DABCO)V_6O_{14}\cdot H_2O$,[26,27] $(en_2M)V_6O_{14}$ (M=Zn, Cu)[28] and $(TMA)V_3O_7$.[33] Crystallographic analysis shows that they differ in the relative orientation of the SP chains and in the way the tetrahedra share their corners. The conformation of the SP chain along with tetrahedra that are attached by two corners (SP_2T) is the same in all cases. However, the final structure is determined by which of the two remaining tetrahedral corners is used to attach to the neighboring SP chain. When the oxygen atom which lies in the same plane as the SP bases is shared, the V_3O_7 layer is flat [Fig. 6(c), (d)]. When the other oxygen is shared [Fig. 6(a), (b)] the layer is tilted and the distance between the chains is significantly shorter, for example 7.597 Å in MAV_3O_7 compared with 8.427 Å in $TMAV_3O_7$. This tilting allows the

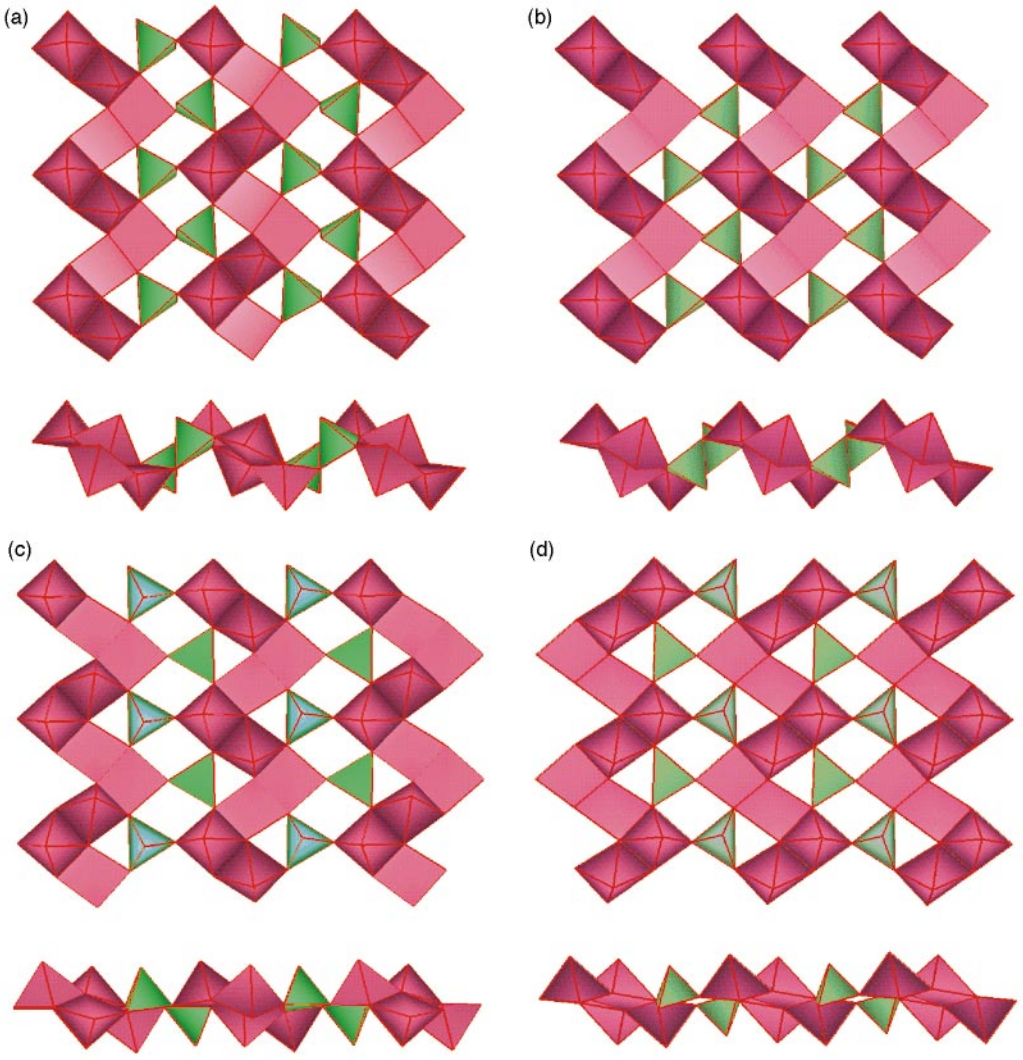

Fig. 6 The structures of vanadium oxide layers of (a) $(CH_3NH_3)V_3O_7$, (b) $(DABCO)V_6O_{14}\cdot H_2O$, (c) $(en_2M)V_6O_{14}$, and (d) $(TMA)V_3O_7$.

vanadyl oxygens to come closer together allowing hydrogen bonding to the methylammonium ions, or the DABCO ions. In the case of the spherical tetramethylammonium ion the bonding is predominantly ionic, and for the $M(en)_2$ complexes the flat layers allow for octahedral coordination around the metal ion, two apical vanadyl oxygens and the two en groups in the plane.

The second distinguishing feature between the layers is the relative orientation of the neighboring SP_2T chains. In the case of $(DABCO)V_6O_{14}$ and $(TMA)V_3O_7$ they are transformed each into another by a simple translation in the direction perpendicular to the chain so that the repeat distance in that direction is equal to the distance between the chains. The transformation between chains can be more complex than simple translation. For instance in $(MA)V_3O_7$ and $(en_2Zn)V_6O_{14}$ two chains interact by the glide plane perpendicular to the chain—translation and reflection. All these cases are summarized in Table 4, where t is the distance between the chains.

The crystal structure of $(CH_3NH_3)_{0.75}V_4O_{10}\cdot 0.67H_2O$ is also layered but contains a double V_2O_5 layer [Fig. 4(b)]. This type of layer is found in compounds intercalated with metals cations such as Ag^+,[34] K^+,[35,36] Na^+,[37] Zn^{2+} and Fe^{2+},[32,38] and also possibly in xerogel V_2O_5.[39] The methylammonium cation and water molecules are statistically disordered between the vanadium oxide layers, just as reported earlier for the iron tetramethylammonium vanadium oxide.[32,38] This is the first occurrence of the double sheet structure with just an organic cation between the layers. The vanadium polyhedron is a distorted octahedron with double bonded oxygen in one apex and weakly bonded oxygen in the opposite site, with V–O distances of 1.59–1.64 Å and 2.47–2.59 Å respectively. The structure[40] of $Ca(V_{7.6}Fe_{0.7})O_{20}\cdot 4.5H_2O$ is the closest to the title compound; its unit cell is $a=11.680$ Å, $b=3.654$ Å, $c=11.025$ Å and $\beta=105.0°$, which compares with those, $a=11.673$ Å, $b=3.668$ Å, $c=11.095$ Å and $\beta=99.865°$, for $(CH_3NH_3)_{0.75}V_4O_{10}\cdot 0.67H_2O$.

Nickel manganese oxide

Electron microprobe analysis showed that the crystals formed had a rod-like morphology. Chemical analysis of the compound formed indicated a 1:1 ratio of nickel to manganese and the overall composition $NiMnO_3H$. Atomic absorption indicated no measurable lithium in the oxide, but the absence of lithium ions in the reaction medium resulted in less pure material. The thermogravimetric analysis of the manganese nickel oxide $NiMnO_3H$ in oxygen and nitrogen at a heating rate of 3 °C min^{-1} is shown in Fig. 7. In oxygen after the first weight loss of almost 2% the compound formed is the ilmenite form of $NiMnO_3$; some oxygen must be abstracted from the lattice as loss of hydrogen would only lead to a 0.6% loss. After the second weight loss the product had the spinel structure, plus some NiO; formation of $NiO+NiMn_2O_4$ would correspond to an overall weight loss of 5.5% as observed. The weight loss in nitrogen is consistent with the hydrogen being lost in the first step as water by abstraction of oxygen from the lattice, 5.3 *vs.* 5.5 wt.% for $x=1$, followed by formation of $NiO+Mn_3O_4$, 7.6 *vs.* 8.2 wt.%.

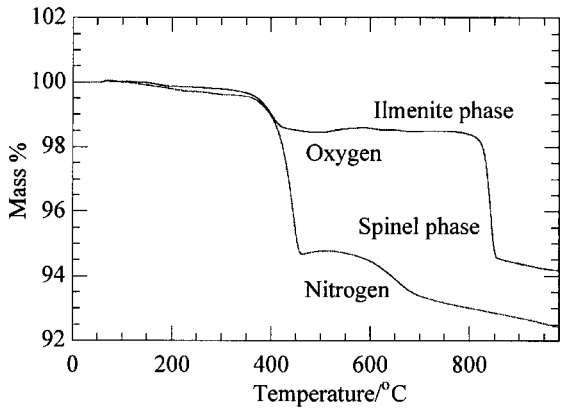

Fig. 7 Thermogravimetric analysis of the nickel manganese oxide $NiMnO_3H$ at a heating rate of 3 °C min^{-1} under oxygen and nitrogen.

The powder X-ray diffractogram, Fig. 8, was quite different from that of the ilmenite phase of the same composition,[41,42] and was indexed as an orthorhombic lattice using the Ito method from CSD software.[43] The structure was solved in space group $Cmc2_1$ by direct methods using integrated intensities in the range 5 to 70° 2θ. The neutron powder pattern was used to verify the crystallographic ordering between Ni and Mn which is suggested by, but cannot be proved from, the X-ray data alone. Final Rietveld refinement was done using the GSAS program[31] simultaneously for both X-ray and neutron sets of data for which observed, calculated and difference plots are shown in Fig. 8(a) and (b) respectively. The high background for the neutron pattern is due to incoherent scattering from the Ni and H, and the poor fit for three reflections (040, 110 and 061) might be due to some magnetic ordering which occurs below 390 K, which is discussed below. Crystallographic parameters are given in Table 5 and atomic parameters and interatomic distances are in Tables 6 and 7 respectively.

The structure of $NiMnO_3H$ is shown in Fig. 9. It comprises layers of nickel oxide and manganese oxide. Nickel is octahedrally coordinated by oxygen. These NiO_6 octahedra form sheets by edge and face sharing. The manganese is in square pyramidal sites with base Mn–O distances of 1.90 and 1.91 Å and an apex distance of 2.11 Å. These MnO_5 square pyramids share edges and corners to form the manganese sheet as shown

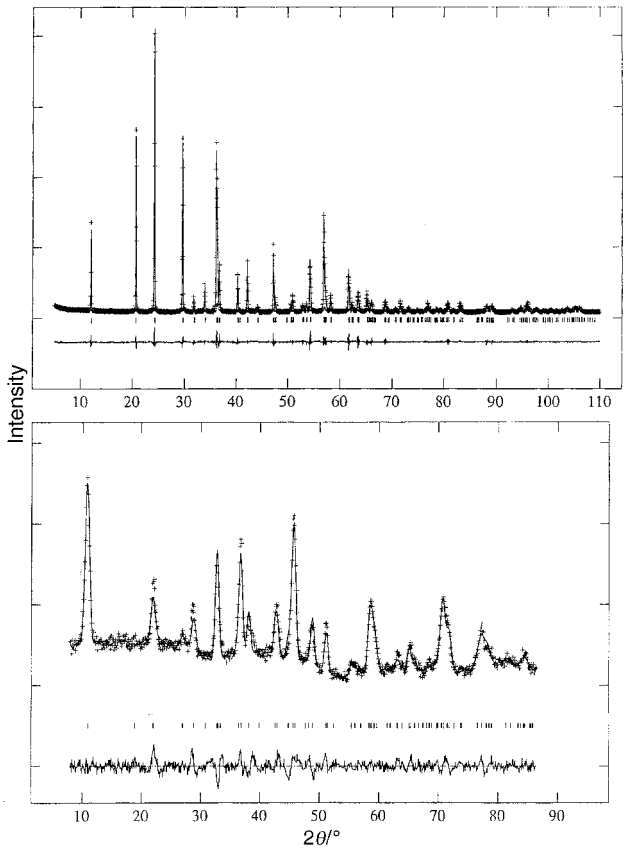

Fig. 8 X-Ray (a) and neutron (b) powder patterns for $NiMnO_3H$. [Observed plot is shown by pluses (grey), calculated plot by solid line. Difference plot appears below. The vertical lines mark reflections.]

Table 5 Experimental details

Crystal data		
Chemical formula	$NiMnO_3H$	
Cell setting	Orthorhombic	
Space group	$Cmc2_1$	
a/Å	2.86089(4)	
b/Å	14.6495(2)	
c/Å	5.27024(5)	
V/Å^{-3}	220.880(5)	
Z	4	
Formula weight	162.7	
D_x/Mg m^{-3}	4.891	
Data collection and refinement		
Diffractometer	Scintag XDS2000	McMaster
Temperature/K	295	295
Radiation type	Cu-Kα	Neutron
Wavelength/Å	1.54178	1.392
Scan method	θ/θ, step scan	$2\theta/\theta$
2θ min/°	5	8
2θ max/°	110	86.4
2θ step/°	0.02	0.1
Exposure time/s	30	20
Peak shape function	Pseudo-Voigt	Gaussian
Preferred orientation	March–Dollase, $(\tau^2\cos^2\phi+\sin^2\phi/\tau)^{-3/2}$	
$R(F^2)$	0.0625	0.0838
R_p	0.0499	0.0306
wR_p	0.0684	0.0394
No. of reflections used	99	82

Table 6 Fractional atomic coordinates and isotropic displacement parameters (Å^2) for $NiMnO_3H$

Atom	x	y	z	U_{iso}
Ni	0	0.9989(3)	0.0	0.0136(5)
Mn	0	0.30538(7)	0.762(1)	0.0149(5)
O1	0	0.4483(3)	0.266(4)	0.007(1)
O2	0	0.1089(2)	0.258(4)	0.006(1)
O3	0	0.2688(3)	0.372(1)	0.023(2)
H	0	0.386(3)	0.391(8)	0.05

Table 7 Distances (Å) and angles (°) for $NiMnO_3H$

Ni–O1	2.136(1)×2	Mn–O2	1.903(2)×2
Ni–O1′	2.041(1)×2	Mn–O3	1.888(4)×2
Ni–O2	2.107(2)	Mn–O3′	2.122(8)
Ni–O2′	2.032(2)		
O1–Ni–O1	84.1(6)	O2–Mn–O2	97.5(2)
O1–Ni–O1′	93.38(8)×2	O2–Mn–O3	79.3(3)×2
O1–Ni–O1′	176.1(7)×2	O2–Mn–O3	162.3(9)×2
O1–Ni–O2	81.0(3)×2	O2–Mn–O3′	98.9(7)×2
O1–Ni–O2′	98.2(5)×2	O3–Mn–O3	98.5(3)
O1′–Ni–O1′	89.0(4)	O3–Mn–O3′	98.8(2)×2
O1′–Ni–O2	95.7(5)×2		
O1′–Ni–O2′	85.1(4)×2		
O2–Ni–O2′	178.9(9)		
O1–H	1.13(4)	O1–H···O3	141(4)
O3···H	1.72(4)		

in Fig. 9 (top right). These manganese square pyramids also share corners with nickel octahedra to form the three-dimensional framework with one trigonal prismatic cavity per formula unit. The distance from the center of this cavity to the center of the neighboring oxygens is from 2.1 to 2.3 Å, giving a cavity size of radius of about 0.8 Å. This is about the same size as a lithium ion. These cavities form a tunnel down the a axis, down which small ions should be able to diffuse.

This nickel manganese oxide reacted with only 0.1 Li above 2 V in an electrochemical cell, consistent with predominently Ni^{3+} and Mn^{3+} but with n-butyllithium ($\approx$1 V *vs.* Li) showed the uptake of 0.91 Li per formula unit of $NiMnO_3$ on the sample as prepared. The lithium content was further confirmed

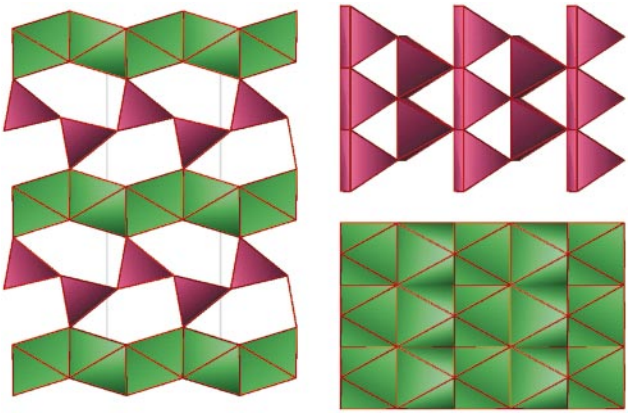

Fig. 9 Structure of the nickel manganese oxide $NiMnO_3$: (left) overall structure, (top right) manganese oxide sheets, and (bottom right) nickel oxide sheets.

by atomic absorption analysis. The intercalated compound $Li_{0.91}NiMnO_3$ appeared to be stable in air. X-Ray diffraction showed no significant change from $NiMnO_3$ itself. This composition is consistent with a lithium ion entering each of the vacant cavities in the $NiMnO_3$ structure possibly displacing hydrogen.

The magnetic susceptibility of $NiMnO_3H$ was measured over the temperature range 10 K to 600 K and the results are shown in Fig. 10 plotted as χ^{-1}. Note that the Curie–Weiss law appears to hold above 400 K. Two transitions are apparent at 390 K and 110 K.

The inverse susceptibility data were fitted to a modified Curie–Weiss function including a temperature independent term, (TIP):

$$\chi = C/(T-\theta)+(\mathrm{TIP})$$

with fitting constants $C=3.43(6)$ emu K mol^{-1}, $\theta=-369(15)$ K and TIP$=2.8\times10^{-4}$ emu mol^{-1}. The large, negative Weiss constant θ indicates that antiferromagnetic interactions predominate. The observed Curie constant, C, can be used to suggest an assignment of the oxidation and spin states for Ni and Mn. The most likely combination possible with relevant spin-only C values are: Ni^{2+} (1.00) and high spin Mn^{3+} (3.00) with some Mn^{4+} (1.87) for $x<1$ in $NiMnO_3H$. However, in view of the Ni/Mn nonstoichiometry, the observed value of the Curie constant is not a reliable indicator of the oxidation and spin states for Ni and Mn in this material. It should be noted that the bond distances of Table 6 are consistent with the assignment Ni^{2+}/Mn^{3+}. This should be verified by XANES, XPS or EELS experiments.

The magnetic properties of this new, orthorhombic form of $NiMnO_3H$ can be compared with the thermodynamically stable ilmenite form. The latter was investigated by Cloud[41] and Pernet *et al.*[42] and shows a single magnetic transition at

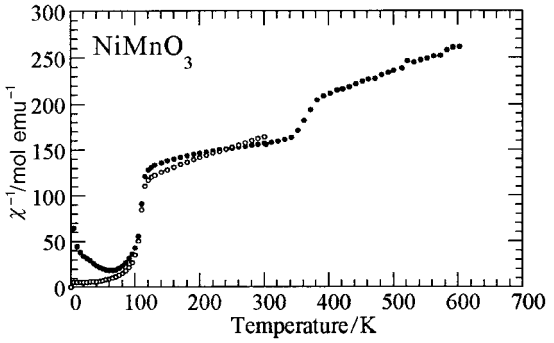

Fig. 10 (a) The inverse of the susceptibility of $NiMnO_3$: ● zero field cooling, and ○ cooled in field.

473 K to a ferrimagnetic structure consisting of ferromagnetic planes of Mn^{4+} and Ni^{2+} moments coupled anti-ferromagnetically. The more complex behavior of the orthorhombic form with two magnetic transitions at lower temperatures cannot presently be understood in detail. The large negative Weiss temperature indicates the predominance of antiferromagnetic couplings but temperature dependent neutron diffraction studies will be necessary to determine the underlying magnetic structures, as demonstrated previously for example for $InMnO_3$.[44] At 5 K the $NiMnO_3H$ sample exhibits a weak spontaneous moment of less than 0.04 μ_B per formula unit suggesting the presence of some form of spin canting.

Conclusions

In conclusion, a new structural form of $NiMnO_3H$ has been formed by a low temperature synthesis approach, where the manganese atoms are in planes containing MnO_5 square pyramids and the nickel atoms in planes containing NiO_6 octahedra. It converts into the known ilmenite form of $NiMnO_3$ at around 400 °C. The structure contains tunnels into which lithium ions can be intercalated. Above 400 K it exhibits paramagnetism with a Curie constant consistent with the presence of predominantly Ni^{2+} and high spin Mn^{3+} ions. Two magnetic phase transitions occur at 390 K and 110 K but the magnetic structures are not known. The methylammonium cation forms several layered vanadates, in which the vanadium coordination decreases with increase of pH of the reaction medium. Hydrogen bonding controls the orientation of the polyhedra in the vanadium sheets, in contrast to the tetramethylammonium ion where the bonding is predominantly ionic.

This research at Binghamton was supported by the National Science Foundation through grant DMR-9810198 and in part by the Department of Energy through the Office of Transportation Technology. We thank Professor Jon Zubieta and Dave Rose at Syracuse University for the use of the Siemens Smart CCD single crystal diffractometer. We also thank Professor Michel Pouchard at the Bordeaux meeting for helpful discussions.

Note added in proof

Yamamoto[45] reported the synthesis of the compound $NiMnO_2(OH)$, its X-ray diffraction pattern, and decomposition to ilmenite but no magnetic data or indexing of the X-ray data. Our analysis of most of the diffraction lines indicates a phase with $a=2.863(1)$, $b=14.652(3)$, and $c=5.273(2)$ Å. This is clearly the same phase as reported here.

References

1 *Soft Chemistry Routes to New Materials—Chimie Douce*, ed. J. Rouxel, M. Tournoux and R. Brec, Trans Tech Publications, Switzerland, 1994, vol. 152–153.
2 R. M. Barrer, *Hydrothermal Chemistry of Zeolites*, Academic Press, London, 1982.
3 J. W. Johnson, A. J. Jacobson, J. F. Brody and S. M. Rich, *Inorg. Chem.*, 1982, **21**, 3820.
4 R. C. Haushalter, K. G. Strohmaier and F. W. Lai, *Science*, 1989, **246**, 1289.
5 J. R. Günter, M. Amberg and H. Schmalle, *Mater. Res. Bull.*, 1989, **24**, 289.
6 K. P. Reis, A. Ramanan and M. S. Whittingham, *Chem. Mater.*, 1990, **2**, 219.
7 K. P. Reis, A. Ramanan and M. S. Whittingham, *J. Solid State Chem.*, 1992, **96**, 31.
8 K. P. Reis, E. Prince and M. S. Whittingham, *Chem. Mater.*, 1992, **4**, 307.
9 J.-D. Guo, P. Zavalij and M. S. Whittingham, *J. Solid State Chem.*, 1995, **117**, 323.
10 J. Guo, P. Zavalij and M. S. Whittingham, *Eur. J. Solid State Chem.*, 1994, **31**, 833.
11 R. Chen, P. Zavalij and M. S. Whittingham, *Chem. Mater.*, 1996, **8**, 1275.
12 R. Chen, T. Chirayil and M. S. Whittingham, *Proceedings of the 10th International Symposium on Solid State Ionics, Singapore, December 1995, Solid State Ionics*, 1996, **86–88**, 1.
13 R. Chen, P. Y. Zavalij and M. S. Whittingham, *Mater. Res. Soc. Symp. Proc.*, 1997, **453**, 653.
14 M. S. Whittingham and F. R. Gamble, *Mater. Res. Bull.*, 1975, **10**, 363.
15 R. Chen and M. S. Whittingham, *J. Electrochem. Soc.*, 1997, **144**, L64.
16 J. S. Beck, J. C. Vartuli, W. J. Roth, M. E. Leonowicz, C. T. Kresge, K. D. Schmitt, C. T.-W. Chu, D. H. Olson, E. W. Sheppard, S. B. McCullen, J. B. Higgins and J. L. Schlenker, *J. Am. Chem. Soc.*, 1992, **114**, 10 834.
17 P. Zavalij, J. Guo, M. S. Whittingham, R. A. Jacobson, V. Pecharsky, C. Bucher and S.-J. Hwu, *J. Solid State Chem.*, 1996, **123**, 83.
18 J. Guo, P. Zavalij and M. S. Whittingham, *Chem. Mater.*, 1994, **6**, 357.
19 Y. J. Li and M. S. Whittingham, *Solid State Ionics*, 1993, **63**, 391.
20 M. S. Whittingham, J. Li, J. Guo and P. Zavalij, *Mater. Sci. Forum*, 1994, **152–153**, 99.
21 M. S. Whittingham, J. Guo, R. Chen, T. Chirayil, G. Janauer and P. Zavalij, *Solid State Ionics*, 1995, **75**, 257.
22 T. A. Chirayil, P. Y. Zavalij and M. S. Whittingham, *Chem. Commun.*, 1997, 33.
23 T. Chirayil, P. Y. Zavalij and M. S. Whittingham, *J. Mater. Chem.*, 1997, **7**, 2193.
24 B. E. Koene, N. J. Taylor and L. F. Nazar, *Angew. Chem.*, 1998, in press.
25 J. Livage, *Proc. Lake Louise Composites Meeting*, 1997, in press.
26 L. F. Nazar, B. E. Koene and J. F. Britten, *Chem. Mater.*, 1996, **8**, 327.
27 Y. Zhang, R. C. Haushalter and A. Clearfield, *Chem. Commun.*, 1996, 1055.
28 Y. Zhang, J. R. D. DeBord, C. J. O'Connor, R. C. Haushalter, A. Clearfield and J. Zubieta, *Angew. Chem., Int. Ed. Engl.*, 1996, **35**, 989.
29 P. Y. Zavalij, F. Zhang and M. S. Whittingham, *Acta Crystallogr., Sect. B*, 1998, in press.
30 L. G. Akselrud, P. Y. Zavalii, Y. N. Grin, V. K. Pecharsky, B. Baumgartner and E. Wolfel, *Mater. Sci. Forum*, 1993, **133–136**, 335.
31 A. C. Larson and R. B. VonDreele, GSAS, General Structure Analysis System User Guide, Los Alamos National Laboratory, Los Alamos, New Mexico, USA, 1994,
32 F. Zhang, P. Y. Zavalij and M. S. Whittingham, *Mater. Res. Bull.*, 1997, **32**, 701.
33 P. Y. Zavalij, T. Chirayil and M. S. Whittingham, *Acta Crystallogr., Sect C.*, 1997, **53**, 879.
34 S. Andersson, *Acta Chem. Scand.*, 1965, 1371.
35 Y. Oka, T. Yao and N. Yamamoto, *J. Mater. Chem.*, 1995, **5**, 1423.
36 J.-M. Savariault and J. Galy, *J. Solid State Chem.*, 1992, **101**, 119.
37 Y. Kanke, K. Kato, E. Takayama-Muromachi and M. Isobe, *Acta Crystallogr., Sect. C*, 1990, **46**, 536.
38 F. Zhang, P. Y. Zavalij and M. S. Whittingham, *Mater. Res. Soc. Symp. Proc.*, 1998, **496**, 367.
39 T. Yao, Y. Oka and N. Yamamoto, *Mater. Res. Bull.*, 1992, **27**, 669.
40 H. T. Evans, J. E. Post and J. A. Nelen, *Can. Mineral.*, 1995, **5**, 1423.
41 W. H. Cloud, *Phys. Rev.*, 1958, **111**, 1046.
42 M. Pernet, J. C. Joubert and B. Ferrand, *Solid State Commun.*, 1975, **16**, 503.
43 L. G. Akselrud, P. Y. Zavalij, Y. N. Grin, V. K. Pecharsky, R. Baumgartner and E. Wolfel, *Mater. Sci. Forum*, 1989, **133**, 335.
44 J. E. Greedan, M. Bieringer, J. F. Britten, D. M. Giaquinta and H.-C. Z. Loye, *J. Solid State Chem.*, 1995, **116**, 118.
45 N. Yamamoto, *J. Jpn. Soc. Powder Metallurgy*, (*in Japanese*), 1986, **33**, 48.

Paper 8/05312J